Supplemental material to this article can be found at:
http://dmd.aspetjournals.org/content/suppl/2022/05/07/dmd.122.000836.DC1

1521-009X/50/7/980–988$35.00
DRUG METABOLISM AND DISPOSITION
dx.doi.org/10.1124/dmd.122.000836
Drug Metab Dispos 50:980–988, July 2022

Sinusoidal Uptake Determines the Hepatic Clearance of Pevonedistat (TAK-924) as Explained by Extended Clearance Model

Philip Sandoval, Bei-Ching Chuang, Lawrence Cohen, Tomoki Yoneyama, Sandeepraj Pusalkar[1], Robert W. Yucha, Swapan K Chowdhury[2], and Paresh P. Chothe[S]

Global Drug Metabolism and Pharmacokinetics, Takeda Development Center Americas, Inc. (TDCA), Lexington, Massachusetts

Received January 20, 2021; accepted April 18, 2021

ABSTRACT

Quantitative assessment of hepatic clearance (CL_H) of drugs is critical to accurately predict human dose and drug-drug interaction (DDI) liabilities. This is challenging for drugs that involve complex transporter-enzyme interplay. In this study, we demonstrate this interplay in the CL_H and DDI effect in the presence of CYP3A4 perpetrator for pevonedistat using both the conventional clearance model (CCM) and the extended clearance model (ECM). In vitro metabolism and hepatocyte uptake data showed that pevonedistat is actively transported into the liver via multiple uptake transporters and metabolized predominantly by CYP3A4 (88%). The active uptake clearance ($CL_{act,inf}$) and passive diffusion clearance ($CL_{diff,inf}$) were 21 and 8.7 ml/min/kg, respectively. The $CL_{act,inf}$ was underpredicted as Empirical Scaling Factor of 13 was needed to recover the in vivo plasma clearance (CL_{plasma}). Both CCM and ECM predicted CL_{plasma} of pevonedistat reasonably well (predicted CL_{plasma} of 30.8 (CCM) and 32.1 (ECM) versus observed CL_{plasma} of 32.2 ml/min/kg). However, both systemic and liver exposures in the presence of itraconazole were well predicted by ECM but not by CCM (predicted pevonedistat plasma area under the concentration-time curve ratio (AUCR) 2.73 (CCM) and 1.23 (ECM))., The ECM prediction is in accordance with the observed clinical DDI data (observed plasma AUCR of 1.14) that showed CYP3A4 inhibition did not alter pevonedistat exposure systemically, although ECM predicted liver AUCR of 2.85. Collectively, these data indicated that the hepatic uptake is the rate-determining step in the CL_H of pevonedistat and are consistent with the lack of systemic clinical DDI with itraconazole.

SIGNIFICANCE STATEMENT

In this study, we successfully demonstrated that the hepatic uptake is the rate-determining step in the CL_H of pevonedistat. Both the conventional and extended clearance models predict CL_{plasma} of pevonedistat well however, only the ECM accurately predicted DDI effect in the presence of itraconazole, thus providing further evidence for the lack of DDI with CYP3A4 perpetrators for drugs that involve complex transporter-enzyme interplay as there are currently not many examples in the literature except prototypical OATP substrate drugs.

Introduction

Many drugs are cleared via hepatic disposition involving phase I and phase II metabolic pathways; therefore, liver microsomes, liver S9 fractions, and primary hepatocytes are widely considered in measuring intrinsic metabolic clearance to predict human hepatic clearance of drugs. However, the liver is a complex organ involving interplay between different processes such as sinusoidal uptake, sinusoidal efflux, metabolism and biliary secretion to drive overall disposition of drugs. Thus, understanding of these individual processes is not only important to accurately predict hepatic clearance (CL_H) of drugs but also to reliably assess drug-drug interaction (DDI) liabilities. With recent advances in the drug transporter field, it has become apparent that uptake transporters at the sinusoidal membrane of hepatocytes play an important role in the hepatic clearance of drugs (Giacomini et al., 2010; Hillgren et al., 2013). Of note, organic anion transporting polypeptides (OATPs), organic anion transporter 2 (OAT2) and organic cation transporter 1 (OCT1) are shown to play an important role in the hepatic clearance of their substrate drugs, such as atorvastatin (Maeda et al., 2011), fluvastatin (Watanabe et al., 2010), cerivastatin (Shitara, 2011), repaglinide (Varma et al., 2013), bosentan (Sato et al., 2018) (OATP substrates), tolbutamide (OAT2 substrate) (Bi et al., 2018b), warfarin (OAT2 substrate) (Bi et al., 2018a) and GNE1 (OCT1 substrate) (Fan et al., 2016).

Generally, hepatic clearance of compounds that are highly permeable and predominantly cleared via metabolism by enzymes is estimated by the conventional clearance model (CCM) (Pang et al., 2019). However, when a compound is a dual substrate of metabolic enzymes and uptake transporters, the extended clearance model (ECM) has been proven to

This research was funded by Millennium Pharmaceuticals, Inc., Cambridge, MA, USA, a wholly owned subsidiary of Takeda Pharmaceutical Company Limited. This work received no external funding.

All authors are current or former employees of Takeda Development Center Americas, Inc. (TDCA), Lexington, MA, USA. All the authors (except Sandeepraj Pusalkar) declares that they hold common stocks in Takeda Pharmaceutical Company Limited.

[1]Current affiliation: Servier Pharmaceuticals, Boston, Massachusetts.
[2]Current affiliation: Boston Pharmaceuticals, Cambridge, Massachusetts.

dx.doi.org/10.1124/dmd.122.000836.
[S] This article has supplemental material available at dmd.aspetjournals.org.

ABBREVIATIONS: AUC, area under the curve; AUCR, area under the concentration-time curve ratio; BSA, bovine serum albumin; CCM, conventional clearance model; $CL_{active,inf}$, active uptake clearance; $CL_{diff,inf}$, passive diffusion clearance; CL_H, hepatic clearance; CL_{plasma}, plasma clearance; CsA, cyclosporine A; DDI, drug-drug interaction; ECM, extended clearance model; ENT, equilibrative nucleoside transporter; ESF, empirical scaling factor; HLM, human liver microbiome; HSA, human serum albumin; K_m, transporter affinity; LC/MS/MS, liquid chromatography tandem mass spectrometry; NBMPR, nitrobenzylthioinosine; NTCP, Na^+-taurocholate co-transporting polypeptide; OATP, organic anion transporting polypeptide; OCT, organic cation transporter; PK, pharmacokinetics; RDS, rate-determining step; TCA, taurocholate.

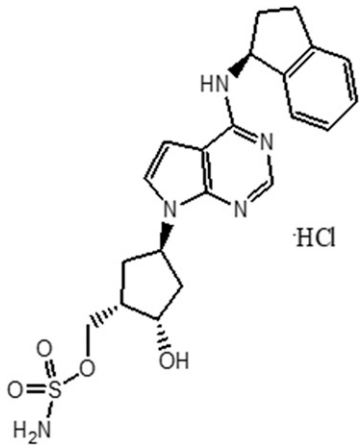

Fig. 1. The chemical structure of pevonedistat.

be quite useful in predicting hepatic clearance as this model accounts for all the individual processes such as uptake clearance, metabolic clearance and biliary clearance that can be involved in the hepatic clearance of a compound (Fujino et al., 2018; Patilea-Vrana and Unadkat, 2018) (eq. 1). The ECM has been shown to be a useful tool in identifying the rate-determining step (RDS) in the systemic clearance of a drug and in predicting DDI liabilities (transport, metabolism or both) (Kunze et al., 2015; Liang and Lai, 2021). Recent clinical data have demonstrated OATP-mediated uptake as the RDS in the hepatic CL of many drugs that are dual substrates of CYP3A4 and OATPs, including atorvastatin, cerivastatin, repaglinide, and bosentan. The area under the curve (AUC) of atorvastatin was increased 12-fold when given with rifampicin (an OATP inhibitor), but it did not change when co-administered with itraconazole (CYP3A4 inhibitor) (Maeda et al., 2011). Similarly, rifampicin increased the AUC of bosentan (3.2-fold), repaglinide (1.9-fold), and simeprevir (7.2-fold), but itraconazole had minimal or no effect on the AUC of these drugs (Yoshikado et al., 2017). This clinical evidence clearly signifies that OATP inhibition, not CYP3A inhibition, has direct influence on the systemic CL of drugs that involve enzyme-transporter interplay where hepatic uptake becomes an RDS.

Pevonedistat is a first-in-class, small molecule inhibitor of neural precursor cell expressed, developmentally down-regulated 8-activating enzyme and currently under investigation for the treatment of malignancies (Bhatia et al., 2016; Swords et al., 2018; Lockhart et al., 2019). The chemical structure of pevonedistat is provided in Fig. 1. Based on available in vitro and in vivo studies, the hepatic metabolism via the CYP3A4 pathway appears to be the primary route of its elimination (Zhou et al., 2021a). Given the major role of CYP3A4 in the metabolic CL of pevonedistat, a dedicated clinical DDI study was conducted with a moderate and a strong CYP3A4 inhibitor, fluconazole and itraconazole, respectively (Faessel et al., 2019). Pevonedistat was administered at 8, 15, and 20 mg/m^2 intravenously in the absence (Day 1) or presence (Day 8) of itraconazole at 200 mg oral single dose (for 7 days). The results from this study indicated that there was no clinically relevant impact of CYP3A4 inhibition (either by itraconazole or fluconazole) on the plasma exposure of pevonedistat as the increase in the dose-normalized AUC was only 1.11-fold and 1.14-fold in the presence of fluconazole and itraconazole, respectively (Faessel et al., 2019). The lack of clinically relevant DDI in plasma in the presence of itraconazole suggested that the hepatic uptake may be the RDS in the hepatic CL of pevonedistat. Therefore, the objective of this study was 3-fold: 1) to comprehensively characterize the hepatic uptake of pevonedistat using cryopreserved primary human hepatocytes, 2) evaluate both the conventional and static extended clearance models to predict the hepatic CL of pevonedistat, and 3) evaluate the application of both these models in predicting DDI with CYP3A4 inhibition.

Materials and Methods

Transporter-qualified cryopreserved human hepatocyte lots (1964, 8280, 8317, 8339, and 8350) were purchased from ThermoFisher Scientific (Waltham, MA USA) (Supplemental Table 1). Human cDNA-expressed rCYPs (Supersomes) were purchased from Corning (Woburn, MA, USA). Heart microsomes (single female donor), lung microsomes (smokers and non-smokers; pooled from 4 donors each [male and female]), and pooled liver microsomes (pooled from 200 donors [male and female]) were purchased from Sekisui-XenoTech (Lenexa, KS, USA). Williams' E medium, cryopreserved hepatocyte recovery medium, hepatocyte maintenance, and plating supplement pack were purchased from ThermoFisher (Waltham, MA USA). Atorvastatin, rifamycin SV (RFV), cyclosporin A, verapamil, ketoprofen and S-(4-Nitrobenzyl)-6-thioinosine (NBMPR), sumatriptan, taurocholic acid (TCA), and uridine were obtained from Sigma-Aldrich(St. Louis, MO USA). [^{3}H]uridine was purchased from Perkin-Elmer (Hopkinton, MA USA). [^{3}H]atorvastatin, [^{3}H]TCA, [^{3}H]sumatriptan, and [^{14}C]tolbutamide were purchased from American Radiolabeled Chemicals, Inc. (St. Louis, MO USA). Pevonedistat and [^{14}C]pevonedistat were prepared and supplied by Millennium Pharmaceuticals, Inc. (Cambridge, MA, USA), a wholly owned subsidiary of Takeda Pharmaceutical Company Limited. All organic solvents were of the highest quality and procured from ThermoFisher (Waltham, MA USA) and Sigma-Aldrich (St. Louis, MO USA).

In Vitro Metabolism Studies

Metabolic Stability Assessment Using Human Liver Microsomes. Pevonedistat (0.1 μM) was incubated with human heart, liver, and lung (smokers and nonsmokers) microsomes (0.5 mg/ml). The incubations were conducted in triplicate in 0.1M potassium phosphate buffer supplemented with or without 2 mM of NADPH and 3 mM of $MgCl_2$, pH 7.4, at 37°C, over 0, 3, 7, 12, 20, and 30 minutes. The reactions were terminated by addition of 90 μl of 0.1 μM of d_8-pevonedistat (internal standard) in acetonitrile. The plates were kept in a freezer for a minimum of 30 minutes for maximal protein precipitation and then centrifuged at 3100 × g at 2°C for 10 minutes. A 75 μl aliquot of the supernatant was then further diluted with 150 μl of water prior to analysis by liquid chromatography and tandem mass spectrometry (LC/MS/MS). The disappearance of pevonedistat over time was monitored by LC/MS/MS.

In vitro Cytochrome P-450 Mapping and Reaction Phenotyping. To determine the CL of pevonedistat in recombinant CYPs, pevonedistat (0.1 μM) was incubated with recombinant CYP1A1, 1A2, 2B6, 2C8, 2C9, 2C19, 2D6, 2J2, 3A4, and 3A5 (20 pmol/ml). The total protein concentration was adjusted to 0.5 mg/ml with appropriate control Supersomes with either P450 oxidoreductase or with both P450 oxidoreductase and cytochrome b_5. The reactions were performed using the same procedure as described above for microsomes.

Uptake Assay in Plated Hepatocytes. Transporter-qualified cryopreserved human hepatocytes (Lots 1964, 8280, 8317, 8339, and 8350) were obtained from ThermoFisher Scientific (Waltham, MA, USA). Cryopreserved hepatocytes were thawed using cryopreserved hepatocyte recovery medium (Life Technologies Corporation) and centrifuged at 100×g for 10 minutes at room temperature. The cell pellets were suspended in William's Medium E (Invitrogen [Carlsbad, CA, USA]) containing 0.1 mM of nonessential amino acids, 2 mM of L-glutamine, 4.5-g/L of glucose, 10% fetal bovine serum (FBS), insulin-transferrin-selenium (1×) (Gibco), 0.1 μM of dexamethasone, and 100 unit/ml of penicillin/streptomycin. The viability of the hepatocytes was determined by a CelloMeter (Nexcelom Bioscience) (Lawrence, MA, USA) and an acridine orange/propidium iodide (AO/PI) staining solution (Nexcelom Bioscience). The hepatocytes were seeded at a density of 0.15 to 0.2 million cells per well onto 48-well plates precoated with Collagen I (Corning Life Sciences, Corning, NY, USA). The hepatocytes were allowed to attach at 37°C for approximately 1 hour with 95% air and 5% CO_2, and the medium was replaced by William's Medium E containing 0.1 mM of nonessential amino acids, 2 mM of L-glutamine, 4.5 g/L of glucose, insulin-transferrin-selenium (1×), 0.1-μM dexamethasone, and 100 unit/mL of penicillin/streptomycin. The hepatocytes were further incubated at 37°C for an additional 3 to 4 hours before use in the assay.

To initiate the uptake assay, hepatocytes were incubated with warm Krebs-Henseleit (KH) buffer for 10 minutes at 37°C. [^{14}C]pevonedistat was then added to hepatocytes at 1 μM. The total uptake of pevonedistat into hepatocytes was measured for 1, 2, 3, 5, 7, and 10 minutes at 37°C. Similarly, the uptake via passive diffusion into hepatocytes was measured at 1 μM for 1, 2, 3, 5, 7, and 10 minutes at 4°C. For inhibition studies, hepatocytes were pre-incubated with an inhibitor for 15 minutes and then co-incubated with an inhibitor and [^{14}C]pevonedistat or a probe substrate for 5 minutes in KHB buffer at 37°C. Rifamycin SV (20 μM), cyclosporine A (CsA, 20 μM), verapamil (300 μM), ketoprofen (300 μM), and nitrobenzylthioinosine (NBMPR, 10 μM) were used as inhibitors for organic anion-transporting polypeptides (OATPs), Na^+-taurocholate co-transporting polypeptide (NTCP) (in addition to OATPs), organic cation transporter (OCT) 1 (also inhibits P-gp), organic anion transporter (OAT) 2, and equilibrative nucleoside transporter (ENT) 1, respectively. We also included rifamycin SV at 1 mM as a pan-inhibitor, which has been shown to inhibit all six major uptake transporters (OATP1B1, OATP1B3, OATP2B1, NTCP, OCT1, and OAT2) (Chothe et al., 2018; Bi et al., 2019). For uptake kinetic experiments, hepatocytes were incubated with pevonedistat at various concentrations (0.27 to 200 μM, [^{14}C]pevonedistat + cold pevonedistat) for 5 minutes. To investigate the effect of human serum albumin (HSA) on pevonedistat uptake, hepatocytes were incubated with pevonedistat (0.45 μM) in KHB buffer and Na+-free buffer (with and without cyclosporine A) containing 0.5% HSA for 3 minutes. At the end of the uptake period, hepatocytes were washed 3 times with ice-cold KHB buffer. The cells were lysed with Triton X-100 (Sigma-Aldrich Company, LLC, St Louis, MO, USA) (0.5%, v:v) in PBS. The samples of radiolabeled substrates were placed into a 96-well Wallac Isoplate (PerkinElmer Life Sciences [Waltham, MA, USA]) and mixed with Ultima-Flo M liquid scintillation cocktail (PerkinElmer Life Sciences [Waltham, MA, USA]). The radioactivity in the samples was measured with a 2450 MicroBeta2 TriLux microplate scintillation and luminescence counter (PerkinElmer Life Sciences [Waltham, MA, USA]). Radioactivity of the dosing solution was used to calculate the initial donor concentration of the substrate. Non-radiolabeled substrates were quantified by liquid chromatography mass spectrometry. The total protein concentration in cell lysates were quantified using the Pierce bicinchoninic acid protein assay (ThermoFisher Scientific, Inc. [Rockford, IL, USA]), with bovine serum albumin (BSA) as the reference standard. The cellular accumulation of pevonedistat and other transporter probe substrates were normalized to the total protein concentration. All experiments were conducted in triplicate ($n = 3$).

Measurement of Protein Abundance of Major Drug Transporter Proteins in Human Hepatocytes by Quantitative Proteomics Using nano LC-MS/MS. The absolute protein abundance of major liver drug transporters in human hepatocyte lots 8317, 8339, and 8350 was measured by targeted proteomics approach using nano LC-MS/MS by Dr. Philip Smith at the University of North Carolina, Chapel Hill. The procedure of membrane preparation, trypsin digestion, and bioanalysis by LC-MS/MS was used as described previously (Khatri et al., 2019; Chothe et al., 2021).

Data Analysis. The time course uptake data of pevonedistat at 37°C and 4°C was fitted with linear regression in GraphPad Prism 8 software (Graphpad Corp, La Jolla, CA, USA) to determine slopes. The uptake inhibition data were analyzed by ordinary one-way ANOVA using Tukey's multiple comparisons test. The active uptake kinetic parameters (K_m and V_{max}) were determined by using Michael Mentalis equation in GraphPad Prism 8 software as described in eq. 1 below.

$$V = \frac{V_{max} \times S}{K_m + S} \quad (1)$$

where V is the uptake rate, V_{max} is the maximum transport velocity, K_m is the affinity of a substrate, and S is the substrate concentration. The passive diffusion clearance ($CL_{diff,inf}$) was determined from the mean of passive diffusion clearance at each concentration of pevonedistat at 4°C.

The hepatic clearance was estimated by the well-stirred clearance model using the following equation:

$$CL_H = Q_H \times \frac{f_u \cdot R_b \times CL_{int}}{Q_H \cdot R_b + f_u \times CL_{int}} \quad (2)$$

where CL_H is plasma-based hepatic clearance, Q_H is liver blood flow (86 L/h), f_u is fraction unbound in plasma, R_b is blood to plasma ratio and CL_{int} is intrinsic clearance. The CL_H of pevonedistat in the presence of itraconazole was determined by using the fraction inhibited by itraconazole of CYP3A4-mediated clearance of pevonedistat (0.88).

Intrinsic hepatic clearance of pevonedistat was estimated using the conventional clearance model (CCM) and extended clearance model (ECM) as described by the following equations, respectively:

$$CL_{int,CCM} = ESF \times (CL_{int,met} + CL_{int,bile}) \quad (3)$$

$$CL_{int,ECM} = (ESF \times CL_{act,inf} + CL_{diff,inf}) \times \frac{CL_{int,met} + CL_{int,bile}}{(CL_{act,eff} + CL_{diff,eff}) + CL_{int,met} + CL_{int,bile}} \quad (4)$$

where CL_{int} is intrinsic clearance, $CL_{int,met}$ is intrinsic metabolic clearance, $CL_{int,bile}$ is intrinsic biliary clearance. $CL_{act,inf}$ and $CL_{diff,inf}$ are the uptake clearances via active and passive diffusion process, respectively, and $CL_{act,eff}$ and $CL_{diff,eff}$ are the efflux via active and passive diffusion process, respectively. $CL_{act,inf}$ is estimated by V_{max}/K_m. Empirical scaling factors (ESF) of 4 and 13 were used to extrapolate in vitro CL_{int} in the CCM and ECM, respectively, to fully recover the vivo plasma clearance of pevonedistat in respective clearance models.

The change in the plasma AUC of pevonedistat in the presence of itraconazole was predicted using following equation:

$$Predicted\ plasma\ AUCR = \frac{CL_H + CL_{renal}}{CL_{H,\,itraconazole} + CL_{renal}} \quad (5)$$

where AUCR is the area under the concentration-time curve ratio of pevonedistat plasma AUC in the absence and presence of itraconazole, CL_H is plasma-based hepatic clearance, CL_{renal} is the renal clearance, and $CL_{H,itraconazole}$ is the plasma-based hepatic clearance of pevonedistat in the presence of itraconazole.

The liver AUC of pevonedistat in the absence and presence of itraconazole was predicted by eqs. 6 and 7, respectively:

$$Predicted\ liver\ AUCR_{CCM} = \frac{Qh + ESF \times (CL_{int,met} + CL_{bile})}{Qh + ESF \times (CL_{int,met,itraconazole} + CL_{bile})} \cdot \frac{CL_H + CL_{renal}}{CL_{H,itraconazole} + CL_{renal}} \quad (6)$$

$$Predicted\ liver\ AUCR_{ECM} = \frac{(Qh \times (CL_{diff,eff} + CL_{int,met} + CL_{bile}) + \frac{fu}{R_b} \times (ESF \times CL_{act,inf} + CL_{diff,inf}) \times (CL_{int,met} + CL_{int,bile})}{(Qh \times (CL_{diff,eff} + CL_{int,met,itraconazole} + CL_{int,bile}) + \frac{fu}{R_b} \times (ESF \times CL_{act,inf} + CL_{diff,inf}) \times (CL_{int,met,itraconazole} + CL_{int,bile})} \cdot \frac{CL_H + CL_{renal}}{CL_{H,itraconazole} + CL_{renal}} \quad (7)$$

where $AUCR_{CCM}$ and $AUCR_{ECM}$ is the ratio of pevonedistat liver AUC in the absence and presence of itraconazole, using the CCM and ECM, respectively,

f_u is plasma unbound fraction, Q_h is liver blood flow, R_b is blood to plasma partitioning ratio, $CL_{act,inf}$ is active uptake clearance, $CL_{diff,inf}$ is passive diffusion clearance, $CL_{int,met}$ and $CL_{int,met,itraconazole}$ is metabolic CL in the absence and presence of itraconazole, CL_{bile} is biliary clearance, and CL_{bile} is renal clearance.

For scaling, metabolic CL of pevonedistat using HLMs following physiologic scalars were used: 40 mg microsomal protein per gram of liver, 21.4 g of liver per kg of body weight and 70 kg of bodyweight: and for the scaling of uptake, CL using human hepatocytes following physiologic scalars were used: 0.657 mg of protein per million cells (Sohlenius-Sternbeck, 2006), 139 million cells per gram of liver, 21.4 g of liver per kg of body weight, and 70 kg of body weight.

Results

In vitro Metabolic Stability of Pevonedistat using HLMs. The in vitro intrinsic metabolic CL of pevonedistat was obtained using HLMs. The CL_{int} value of pevonedistat was 51.1 μl/min/mg protein at concentration of 0.1 μM. The measured non-specific binding ($f_{u,mic}$) of pevonedistat at the protein concentration of 0.5 mg/ml was 0.49. In the same study, the depletion of pevonedistat (0.1 μM) was inhibited by 87.7% following ketoconazole treatment (1 μM). These results suggested that the contribution of CYP3A4 to the CYP-mediated metabolism of pevonedistat is 88% in vitro.

In vitro Cytochrome P-450 Mapping and Reaction Phenotyping of Pevonedistat. The CYP reaction phenotyping of pevonedistat (0.1 μM) was conducted using recombinantly expressed CYP enzymes as described under experimental section. This assessment involved the monitoring of the depletion of pevonedistat over the period of 30 minutes. In addition to hepatic enzymes (CYP1A2, 2A6, 2B6, 2C8, 2C9, 2C19, 2D6, 2E1, 3A4, 3A5, 4F2, 4F3, and 4F12), the role of extrahepatic enzymes and non-cytochrome P450 enzymes was also evaluated. CYP3A4 was found to be the primary enzyme responsible for >90% of the hepatic metabolism of pevonedistat, consistent with the percent inhibition in the presence of ketoconazole in HLM. The data also indicated that, in addition to CYP3A4/5, pevonedistat is metabolized by CYP1A1, 2J2, and 2C8, and to a lesser extent by CYP1A2, 2B6, 2C9, 2C19, and 2D6. The other CYPs, CYP2A6, 2E1, 4F3A, 4F3B, and 4F12, did not contribute to the CL of pevonedistat.

To assess the relative contribution of extrahepatic enzymes (CYP1A1 and CYP2J2) to metabolism of pevonedistat, a preliminary scaling of these recombinant CYP data together with respective tissue CYP abundance values was conducted. The results showed negligible whole-organ CL_{int} in the heart (CYP2J2) and lung (CYP1A1) tissue in comparison with liver (Table 1).

Based on the in vivo radiolabeled absorption, distribution, metabolism, and excretion /mass balance study in cancer patients, the unchanged pevonedistat accounted for approximately 5% and 17% of the administered dose in urine and feces, respectively, following infusion of 25 mg/m^2 of [^{14}C]pevonedistat, indicating minimal contribution from renal and biliary elimination, thus supporting metabolic clearance as the predominant route of elimination of pevonedistat. This was also well supported by in vitro sandwich cultured human hepatocytes in which biliary excretion of pevonedistat was found to be low (data not shown) Pevonedistat $CL_{IV,plasma}$ and CL_{renal} were estimated to be 32.2 L/h and 0.8 L/h, respectively (Zhou et al., 2021a). Thus, based on the in vitro and in vivo metabolism and, mass balance data pevonedistat clearance appeared to be predominantly mediated via metabolism by CYP3A.

Determination of Pevonedistat Uptake in Human Hepatocytes. The uptake of pevonedistat was analyzed at 1 μM at 37°C and 4°C in plated human hepatocytes for two donors, 4317 and 8280, as described under experimental section. The uptake was linear up to 5 minutes and 10 minutes in lot 8317 and lot 8280, respectively. The uptake of pevonedistat was found to be 2- to 3.5-fold higher at 37°C compared with the uptake at 4°C (Fig. 2). The uptake clearance (CL_{inf}) was determined from the slopes of the initial uptake rate-time profile of pevonedistat at 37°C and 4°C for both the lots. The CL_{inf} was 13.98 and 3.98 μl/min/mg protein at 37°C and 4°C, respectively, for the lot 4317 and 16.85 and 8.64 μl/min/mg protein at 37°C and 4°C, respectively, for the lot 8280.

Assessment of Transporter/s Involved in the Hepatic Uptake of Pevonedistat using Pre-Validated Reference Inhibitors. The time course study indicated that pevonedistat is actively transported into human hepatocytes; therefore, we further investigated its uptake to delineate the potential transporter/s involved using known transporter inhibitors in the three lots of human hepatocytes, 4317, 8339, and 8350. We first validated all the reference inhibitors for their selectivity toward respective transporters using transporter-specific probe substrates. We used atorvastatin for OATP1B1/OATP1B3/OATP2B1, taurocholic acid for NTCP, sumatriptan for OCT1, tolbutamide for OAT2, and uridine for ENT1 (Supplemental Fig. 1). As expected, rifamycin SV (20 μM) inhibited atorvastatin uptake by 59% to 94%, CsA (20 μM) inhibited taurocholic acid (TCA) uptake by 80% to 100%, verapamil (300 μM) inhibited sumatriptan uptake by 73% to 83%, ketoprofen (300 μM) inhibited tolbutamide uptake by 85% to 100%, and NBMPR (10 μM) inhibited uridine uptake by 80% to 94% in all three lots of hepatocytes. Rifamycin SV at 1 mM (pan-uptake transporter inhibitor) completely

TABLE 1

Scaling of CL_{int} of pevonedistat from recombinent CYPs

CYP	CL_{int} μl/min/pmol	CYP abundance (pmol/mg)	CL_{int}[a] μl/min/mg	ISEF[b]	CL_{int} L/h	% fm
1A2	0.0744	52	3.87	0.43	13.09	1.4
2B6	0.0835	17	1.42	0.43	4.8	0.5
2C8	0.1040	24	2.5	0.43	8.45	0.9
2C9	0.0599	73	4.37	0.78	26.84	3
2C19	0.0434	14	0.61	0.25	1.2	0.1
2D6	0.0333	8	0.27	0.75	1.8	0.2
3A4/5	3.27	137	448	0.24	846.17	93.5
2J2 (liver)	0.7010	1.2	0.84	0.43	2.85	0.3
2J2 (heart)	0.7010	0.2	0.12	1	0.03	
1A1 (lung)	0.3210	38.9[c]	12.5	1	1.69	

[a] Measured f_{umic} of 0.49 was applied.
[b] The default SimCyp inter-system extrapolation factors (ISEF) for BD-genest supersomes were applied.
[c] Reported (Kim et al., 2004) and (Delozier et al., 2007).

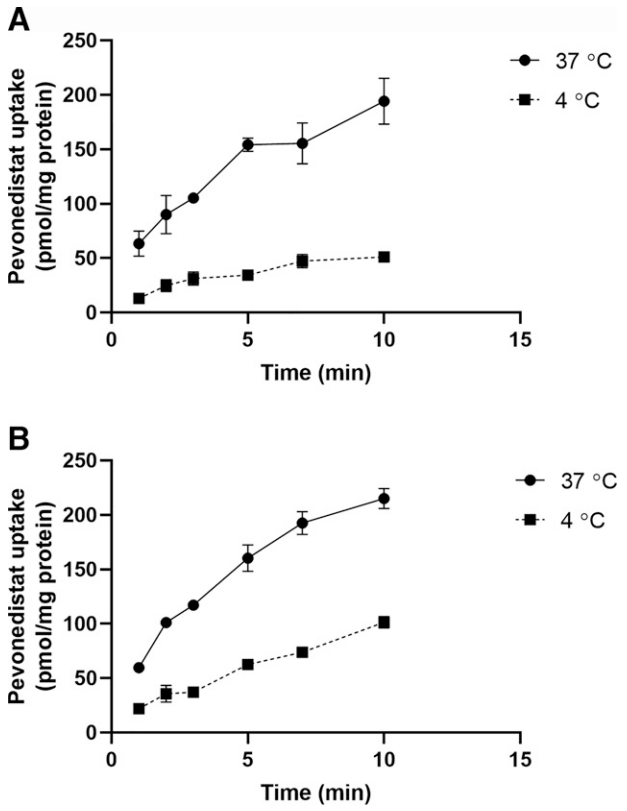

Fig. 2. Time course of pevonedistat uptake in plated human hepatocytes. The uptake of [^{14}C]pevonedistat (1μM) was measured at 37°C and 4°C for 1, 2, 3, 5, 7, and 10 minutes in plated human hepatocyte (A) lot 8317 and (B) 8280. The experiment was done in triplicates (n = 3).

inhibited OATP-mediated atorvastatin uptake (100%), NTCP-mediated TCA uptake (100%), OCT1-mediated sumatriptan uptake (93% to 100%), OAT2-mediated tolbutamide uptake (51% to 100%), and ENT1-mediated uridine uptake (99% to 100%) in all three lots of human hepatocytes.

No significant inhibition of pevonedistat active uptake was observed in the presence of the reference inhibitors; rifamycin SV (20 μM), CsA (20 μM), verapamil (300 μM), ketoprofen (300 μM), and NBMBR (10 μM) in lots 8317, and 8350 while the active uptake of pevonedistat was inhibited 44% by rifamycin SV (20 μM), 43% by CsA (20 μM), 26% by verapamil (300 μM), 37% by ketoprofen (300 μM), and 35% by NBMPR (10 μM) in lot 8339. Additionally, 1 mM of rifamycin SV (a pan-inhibitor) inhibited pevonedistat uptake by 78% and 34% in lots 8339 and 8350, respectively. No inhibition of pevonedistat uptake was observed by 1 mM of rifamycin SV in lot 8317 (Figure 3 and Table 2).

Analysis of HSA Effect on Pevonedistat Uptake in Human Hepatocytes. Recent literature has indicated that the addition of HSA in in vitro transporter studies can improve uptake of drugs that have high nonspecific binding (Miyauchi et al., 2018). Therefore, we examined the effect of 0.5% HSA on pevonedistat in human hepatocytes. The uptake of pevonedistat was measured in KHB buffer and Na^+-free KHB buffer containing 0.5% HSA in the absence and presence of OATP inhibitor cyclosporine A at 37°C and 4°C in human hepatocytes lots 8280 and 8317. Pevonedistat showed active uptake; however, cyclosporine A did not inhibit pevonedistat uptake in the presence of 0.5% HSA (Fig. 4 and Table 4).

Measurement of Uptake Kinetics Parameters of Pevonedistat Uptake in Human Hepatocytes. To investigate the concentration dependence and determine the kinetic parameters of pevonedistat uptake into human hepatocytes, the uptake of pevonedistat within the range of 0.1 to 200 μM was determined at 4°C and 37°C in hepatocyte lots 8280 and 8317. The uptake of pevonedistat was concentration-dependent

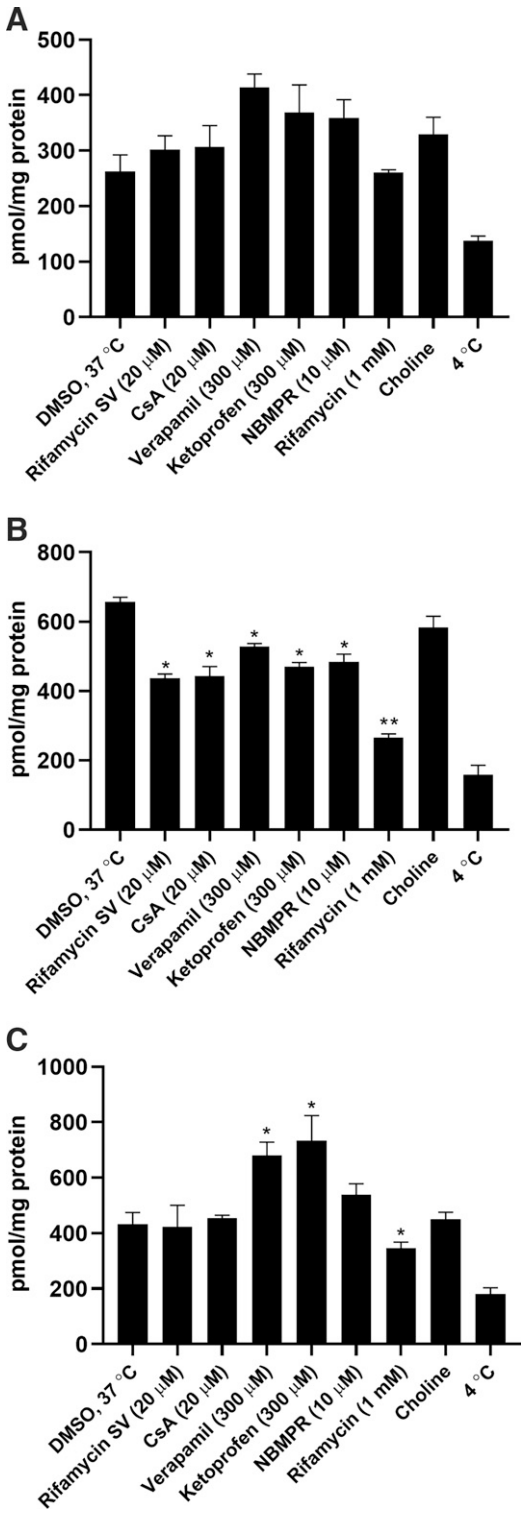

Fig. 3. Inhibition of pevonedistat uptake in plated human hepatocytes. The uptake of [^{14}C]pevonedistat (3μM) was measured at 37°C in the absence and presence of rifamycin SV (20 μM), CsA (20 μM), verapamil (300 μM), ketoprofen (300 μM), NBMPR (10 μM), and rifamycin SV at 1 mM for 5 minutes in plated human hepatocyte lots (A) 8317, (B) 8339, and (C) 8350. The uptake of [^{14}C]pevonedistat (3μM) was also measured at 37°C in the presence of choline buffer (Na^+) and at 4°C in all 3 lots of human hepatocytes. The experiment was done in triplicates (n = 3). Statistical significance * $p < 0.05$ and ** $p < 0.01$.

TABLE 2

Summary of pevonedistat uptake in plated human hepatocytes

Inhibitor	Uptake Rate (pmol/min/mg protein) (mean±SD)			Percent Control (%) (mean±SD)		
	Lot 8317	Lot 8339	Lot 8350	Lot 8317	Lot 8339	Lot 8350
KHB, 37°C	262.5 ± 29.9	657.1 ± 13.3	432.5 ± 42.5	NA	NA	NA
KHB, 4°C	137.2 ± 8.7	158.5 ± 27.2	180.8. ± 22.0	NA	NA	NA
Rifamycin SV (20μM)	301.7 ± 25.1	436.3 ± 12.9	422.9 ± 77.3	131.3 ± 20.0	55.7 ± 2.6	96.2 ± 30.7
CsA (20 μM)	306.8 ± 38.5	443.1 ± 27.5	454.6 ± 9.8	135.3 ± 30.7	57.1 ± 5.5	108.8 ± 3.9
Verapamil (300 μM)	414.2 ± 24.0	528.5 ± 8.6	680.8 ± 47.4	221.1 ± 19.1	74.2 ± 1.7	198.7 ± 18.8
Ketoprofen (300 μM)	368.9 ± 49.7	470.6 ± 11.5	733.2 ± 90.2	184.9 ± 39.7	62.6 ± 2.3	219.5 ± 35.9
NBMPR (10 μM)	358.4 ± 33.5	484.0 ± 22.5	538.4 ± 39.4	176.6 ± 26.7	65.3 ± 4.5	142.1 ± 15.7
Rifamycin SV (1 mM)	260.5 ± 5.2	265.9 ± 10.7	346.6 ± 21.6	98.4 ± 4.2	21.5 ± 2.1	65.9 ± 8.6
Choline	330.0 ± 30.2	582.7 ± 33.2	449.9 ± 25.6	153.9 ± 24.1	85.1 ± 6.7	106.9 ± 10.2

(Fig. 5). The K_m and V_{max} for lot 8280 were 179.3±35.74 μM and 4039±446.4 pmol/min/mg protein, respectively, and the K_m and V_{max} for lot 8317 were 186.5±37.56 μM and 3664±414.7 pmol/min/mg protein, respectively. These parameters were used to determine the $CL_{act,inf}$ of pevonedistat in each lot. The mean of $CL_{act,inf}$ was then used for in vivo extrapolation. Similarly, the mean of $CL_{diff,inf}$ at each concentration of pevonedistat was determined and used a $CL_{diff,inf}$ for in vivo extrapolation (Table 5).

Application of ECM to Predict Hepatic Clearance of Pevonedistat and the DDI Effect in the Presence of Itraconazole on Pevonedistat Plasma Exposure. The CL_H of pevonedistat was determined by both the CCM and ECM using eqs. 3–4. The predicted CL_{plasma} was found to be 30.8 L/h and 32.1 L/h by the CCM and ECM, respectively (Table 5). In the ECM model, the CL_{active} of pevonedistat was scaled using ESF of 13 as it was needed to recover the observed CL_{plasma} of pevonedistat as indicated in Supplemental Fig. 2. Further, we used these models to predict the DDI effect on pevonedistat PK in the presence of itraconazole. The ratio of the plasma and liver AUC of pevonedistat in the absence and presence of itraconazole was predicted using eqs. 5–7. The data are shown in Table 5.

Discussion

Understanding of hepatic disposition of drugs is essential in accurate prediction of hepatic CL, human PK/dose projection, and DDI liabilities. However, this has become challenging due to dynamic interplay between different processes, such as sinusoidal uptake and efflux, metabolism and biliary excretion. Therefore, use of a physiologically relevant model which accounts for all these processes is crucial to accurately predict CL_H and to identify RDS for assessing DDI liabilities during drug development. In such cases, the ECM, which accounts for enzyme-transporter interplay in the hepatic disposition, has been widely used (Kimoto et al., 2018). In this study, we evaluated the ECM in predicting the CL_H of pevonedistat and DDI effect in the presence of CYP3A perpetrator, itraconazole.

First, we characterized the metabolism of pevonedistat using HLMs and CYP phenotyping. These data revealed the major role of CYP3A (f_m = 0.88) in pevonedistat metabolism. This was further confirmed by the in vivo metabolism and mass balance studies (Zhou et al., 2021a) in which approximately 74% of the administered dose cleared via hepatic oxidative metabolism. Based on this evidence, clinical DDI was anticipated with itraconazole, a potent CYP3A4 inhibitor; interestingly however, inhibition of CYP3A4 did not result in a meaningful increase in the systemic exposure of pevonedistat. Previously, a similar phenomenon has been shown for OATP and CYP3A4 substrate drugs where OATP-mediated hepatic uptake is the RDS in their CL_H. Therefore, to explain the reason for the lack of DDI in the presence of itraconazole,

TABLE 3

The protein abundance of drug transporters in human hepatocytes as measured by targeted proteomics

Transporter	pmol/mg protein (Mean ± SD)		
	Lot 8317	Lot 8339	Lot 8350
OATP1B1	3.04 ± 0.13	8.51 ± 0.69	8.59 ± 0.01
OATP1B3	0.33 ± 0.1	1.62 ± 0.63	1.5 ± 0.08
OATP2B1	2.21 ± 0.64	1.4 ± 1.9	2.74 ± 0.7
NTCP	0.18 ± 0.25	0.41 ± 0.5	2.11 ± 0.56
OCT1	2.84 ± 0.08	3.25 ± 0.19	2.32 ± 0.13
OAT2	0.74 ± 0.05	1.04 ± 0.25	1.8 ± 0.17
P-gp	0.23 ± 0.1	0.53 ± 0.55	0.84 ± 0.16
MRP2	1.15 ± 0.05	1.09 ± 0.07	1.96 ± 0.25
Na-K ATPase	10.25 ± 1.3	10.9 ± 0.27	10.2 ± 1.9

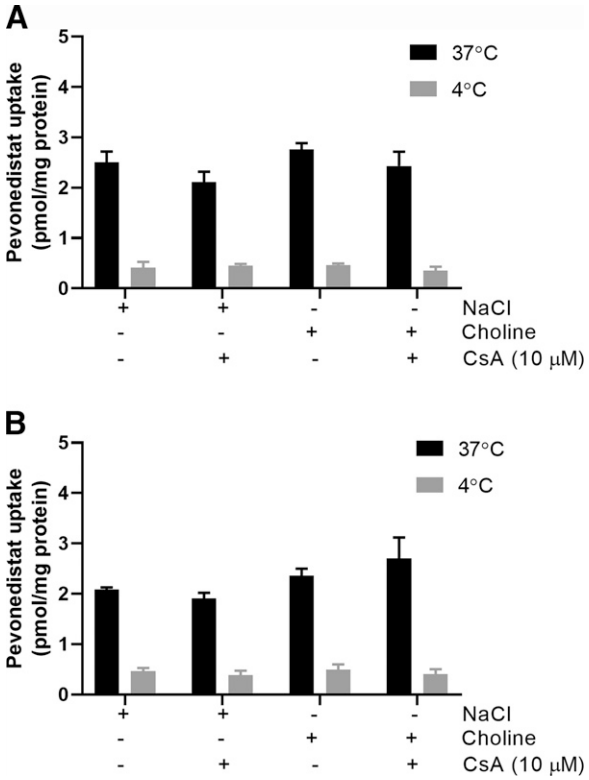

Fig. 4. Effect of HSA on the uptake of pevonedistat in plated human hepatocytes. The uptake of [^{14}C]pevonedistat (0.45μM) was measured at 37°C and 4°C with and without CsA (10 μM) in KHB buffer and choline buffer containing 0.5% HSA in plated human hepatocyte lots (A) 8317 and (B) 8280.

TABLE 4

Uptake rates of pevonedistat in the presence of 0.5% HSA in plated human hepatocytes

	Uptake rate (pmol/min/mg protein)			
	Lot 8317		Lot 8280	
Condition	4°C	37°C	4°C	37°C
KHB buffer, 37°C	0.406 (0.118)	2.50 (0.22)	0.462 (0.066)	2.08 (0.047)
KHB + CsA	0.448 (0.034)	2.11 (0.209)	0.377 (0.092)	1.91 (0.108)
Choline, 37°C	0.457 (0.034)	2.76 (0.125)	0.487 (0.109)	2.36 (0.139)
Choline + CsA	0.352 (0.080)	2.43 (0.285)	0.404 (0.100)	2.70 (0.418)

the uptake of pevonedistat was investigated at 37°C, 4°C and in the presence of selective inhibitors of major liver uptake transporters and a pan-inhibitor (1 mM of rifamycin SV) (Chothe et al., 2018). The uptake of pevonedistat was temperature-dependent and sodium-independent. Interestingly, no significant inhibition of pevonedistat uptake was observed in the presence of reference inhibitors in lots 8317 and 8350; however, rifamycin SV (1 mM) inhibited the uptake by 34% in lot 8350, whereas the uptake was inhibited in the range of 26–44% by OCT1, OATP, OAT2, and ENT1 inhibitors and 78% by 1 mM of rifamycin SV in lot 8339. These data indicated that lot 8339 was the most sensitive to inhibitors. The reason for the lot-to-lot variability in the inhibition of pevonedistat uptake is attributed to different expression levels of drug transporter proteins. The protein abundance data indicated that lot 8317 has significantly lower expression of OATP1B1 (3-fold), OATP1B3 (5-fold), NTCP (2- to 11-fold) and P-gp (2- to 4-fold) compared with lots 8339 and 8350 (Table 3). Therefore, the effect of the pan-inhibitor was more prominent in lots 8339 and 8350 compared with the effect in lot 8317. We also observed an increase in the uptake of pevonedistat in the presence of verapamil and ketoprofen. Verapamil is known to inhibit P-gp that is functionally expressed in plated human hepatocytes (Lundquist et al., 2014). Given pevonedistat as a substrate of efflux transporters (data not shown) it is likely that inhibition of P-gp by verapamil might have increased the uptake of pevonedistat. In 2006, Ishiguro et al. reported that the uptake of telmisartan (high non-specific binding), is greatly improved in the presence of HSA (Ishiguro et al., 2006). Similarly, we analyzed the uptake of pevonedistat with and without CsA in the presence of 0.5% HSA assuming that nonspecific binding of pevonedistat is potentially masking the effect of inhibitors. However, HSA did not improve the inhibition of pevonedistat uptake by CsA (Fig. 4), suggesting nonspecific binding is not interfering with the effects of inhibitors. The binding of CsA to 0.5% HSA is considered to be low as it has been shown to bind to only lipoproteins in human plasma (Wasan et al., 2008). Taken together, these data suggested that the hepatic uptake of pevonedistat is potentially mediated by minor contributions from multiple transporters, such as OATPs, OAT2, and ENT1. Subsequently, we determined $CL_{act,inf}$ and $CL_{diff,inf}$ of pevonedistat using human hepatocytes as they capture all the individual transport processes. Typically, $CL_{act,inf}$ measured using current in vitro tools

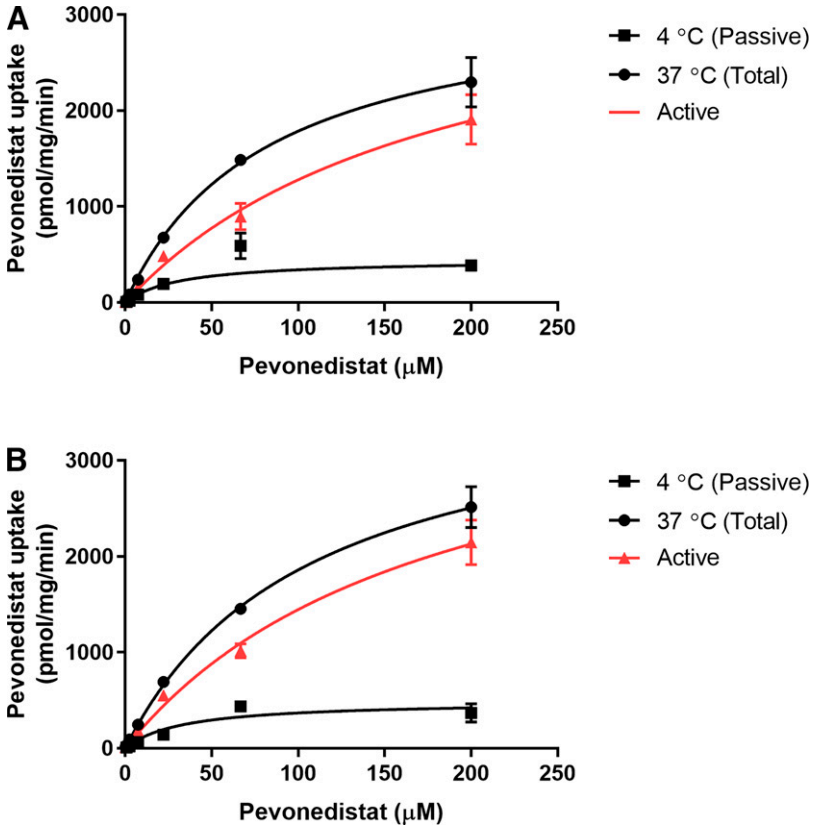

Fig. 5. Uptake kinetics of pevonedistat in plated human hepatocytes. The uptake of [^{14}C]pevonedistat was measured at 37°C and 4°C in KHB buffer at different concentrations ranging from 0.27 to 200 μM in plated human hepatocyte lots (A) 8317 and (B) 8280.

TABLE 5

Input parameters used in predicting hepatic clearance of pevonedistat using ECM

Parameters	CL_{int} (μl/min/10^6 cells)	Predicted CL_{int} (ml/min/kg)	Observed Renal CL (L/h)	Predicted Plasma CL (CCM) (L/h)	Predicted Plasma CL (ECM) (L/h)	Observed Plasma CL (L/h)
Passive efflux ($CL_{diff,eff}$)	2.9	8.7		30.8	32.1	32.2
Active uptake CL ($CL_{act,inf}$)	7.1	21		(ESF 4)	(ESF 13)	
Intrinsic metabolic CL ($CL_{int,met}$)	51.1[a]	43.7	0.8			
Intrinsic biliary CL ($CL_{int,bile}$)	ND	15.1[b]				
Active efflux ($CL_{act,eff}$)	ND	ND				
Passive diffusion CL ($CL_{diff,inf}$)	2.9	8.7				

ND, not determined.
[a] Unit is μl/min/mg of microsomal protein.
[b] Biliary CL was backcalculated from in vivo metabolism and mass balance data.

(hepatocytes and transporter cell lines) is underpredicted (Varma et al., 2014; Chothe et al., 2018). In this study, we also observed significant underprediction of $CL_{act,inf}$ of pevonedistat using human hepatocytes as indicated by the ESF of 13 that was needed for extrapolation to successfully recover the observed CL_{plasma} (Supplemental Fig. 2). This ESF was comparable to the ESF of rosuvastatin (19) that was used as a control in this study (data not shown) and also with the ESF reported in the literature for typical OATP substrates (Varma et al., 2014; Chothe et al., 2018). Interestingly, $CL_{diff,inf}$ measured at 4°C was found to be saturated at higher concentration (200 μM); however, the underlying reason for this effect is unknown and remains to be investigated. Nevertheless, we calculated $CL_{act,inf}$ and $CL_{diff,inf}$ of pevonedistat, excluding the uptake at 200 μM to evaluate the possible impact on in vitro to in vivo extrapolation and DDI prediction (data not shown). The required ESF for in vitro to in vivo extrapolation and prediction of DDI effect was found to be very close to the one using original uptake data indicating minimal impact of saturation on in vitro to in vivo extrapolation and DDI predictions.

In this study, we observed that $CL_{int,met}$ plus $CL_{int,bile}$ of pevonedistat is much greater than its $CL_{diff,inf}$ ($CL_{int,met}$ + $CL_{int,bile}$ of 58.9 ml/min/kg versus $CL_{diff,inf}$ of 8.7 ml/min/kg); therefore, to predict CL_H of pevonedistat, we used the ECM incorporating both CL_{inf} ($CL_{act,inf}$ and $CL_{diff,inf}$) and CL_{met}. With the ESF of 13 for $CL_{act,inf}$, the predicted CL_{plasma} was in good agreement with observed CL_{plasma} (Table 5) of pevonedistat. For comparison, CL_{plasma} was also predicted by the CCM, providing a reasonable prediction of CL_{plasma} (30.8) with an ESF of 4. We later evaluated both the CCM and ECM in terms of their predictivity for DDI between pevonedistat and itraconazole. Importantly, the predicted plasma AUCR of pevonedistat was more than 2-fold higher than the observed plasma AUCR by the CCM, whereas the observed plasma AUCR was closely matched with the predicted AUCR by the ECM (Table 6). In our study, the sinusoidal efflux of pevonedistat was not fully characterized, and it was assumed to be equal to CL_{diff}; however, when we exercised the ECM incorporating sinusoidal efflux the AUCR of pevonedistat was overpredicted (1.83 versus observed AUCR of 1.23), suggesting that sinusoidal CL_{eff} of pevonedistat is minimal. Collectively, these data suggested that both the CCM and ECM models are good in predicting CL_{plasma} of dual substrates of transporters and enzymes; however, the ECM is more appropriate to reliably predict DDI effect and identify RDS such as hepatic uptake.

TABLE 6

Prediction of DDI effect with itraconazole on pevonedistat plasma and liver exposure

Model	Predicted Plasma AUCR	Observed Plasma AUCR	Predicted Liver AUCR
Conventional CL model	2.73	1.14	2.73
Extended CL model	1.23		2.85

Typically, transporter substrate drugs are asymmetrically distributed into the liver due to the concentration gradient developed by uptake transporters (Zhang et al., 2019). In this scenario, any changes in drug concentration inside the liver is not truly reflected in the plasma. This has been well demonstrated in the study by Chang et al., in which OATP-mediated uptake drives the asymmetric distribution of atorvastatin into the liver while CYP3A4 inhibition by itraconazole increases the liver concentration of atorvastatin by 21-fold without any meaningful change in systemic exposure in mice (Chang et al., 2014). Similarly, in our study, the ECM predicted significant impact of itraconazole on the liver exposure (liver AUCR of 2.85) but not on the plasma exposure (plasma AUCR of 1.23) of pevonedistat. These results highlighted the application of the static ECM in characterizing systemic DDI as well as in assessing potential liver DDI risk. Meanwhile, the CCM predicted the similar degree of DDI in both plasma and liver, which is not surprising, as the CCM assumes high permeability between plasma and liver, and systemic DDI serves as a good surrogate of liver DDI.

The modulation of hepatic OATP function significantly impacts the PK of many of its substrate drugs (Giacomini et al., 2010; Yoshikado et al., 2017). For example, significant fractional contribution (ft > 0.9) of OATP1B1 to the uptake of statin drugs (Bi et al., 2019) and repaglinide has been reported and, therefore, OATP inhibition significantly increases systemic exposure of these drugs, particularly statins, to a level causing deleterious effects (Alam et al., 2018). In this study, we were not able to quantitatively estimate the contribution of individual transporters to the hepatic uptake of pevonedistat due to differential sensitivity of hepatocyte donor lots to inhibitors and the weak contribution from individual transporters, indicating lower DDI risk.

In conclusion, the present study provides an important example of the hepatic uptake as an RDS in the CL_H. We demonstrated that although both the ECM and CCM predict CL_H reasonably well, the DDI effect (CYP3A4 inhibition) was successfully explained by the ECM but not CCM for dual substrates of uptake transporter and CYP3A. Recently, we have also developed a physiologically-based pharmacokinetic model with a nested permeability-limited liver model using the Simcyp Population-Based Simulator to describe the hepatic disposition of pevonedistat and the DDI effects with itraconazole (CYP3A4 inhibitor) and rifampicin (OATP inhibitor and CYP3A4 inducer). The details of this model and its application in PK simulation and DDI predictions has been described in the poster presented at the American College of Clinical Pharmacology annual meeting (Zhou et al., 2021b).

Acknowledgments

The authors would like to thank Professor Yuichi Sugiyama (Josai international University) for his input in this work, especially in conducting uptake experiments in the presence of human serum albumin. The authors

also extend their thanks to Drs. Philip C. Smith and John K Fallon at the University of North Carolina, Chapel Hill for their help in conducting targeted proteomics to measure the protein abundance of drug transporters in human hepatocytes.

Authorship Contributions

Participated in research design: Sandoval, Cohen, Pusalkar, Chowdhury, Chothe.

Conducted experiments: Sandoval, Chuang, Cohen, Pusalkar, Yucha.

Performed data analysis: Sandoval, Chuang, Cohen, Yoneyama, Pusalkar, Yucha, Chothe.

Wrote or contributed to the writing of the manuscript: Sandoval, Cohen, Yoneyama, Pusalkar, Chowdhury, Chothe.

References

Alam K, Crowe A, Wang X, Zhang P, Ding K, Li L, and Yue W (2018) Regulation of Organic Anion Transporting Polypeptides (OATP) 1B1- and OATP1B3-Mediated Transport: An Updated Review in the Context of OATP-Mediated Drug-Drug Interactions. *Int J Mol Sci* **19**:855.

Bhatia S, Pavlick AC, Boasberg P, Thompson JA, Mulligan G, Pickard MD, Faessel H, Dezube BJ, and Hamid O (2016) A phase I study of the investigational NEDD8-activating enzyme inhibitor pevonedistat (TAK-924/MLN4924) in patients with metastatic melanoma. *Invest New Drugs* **34**:439–449.

Bi YA, Costales C, Mathialagan S, West M, Eatemadpour S, Lazzaro S, Tylaska L, Scialis R, Zhang H, Umland J, et al. (2019) Quantitative Contribution of Six Major Transporters to the Hepatic Uptake of Drugs: "SLC-Phenotyping" Using Primary Human Hepatocytes. *J Pharmacol Exp Ther* **370**:72–83.

Bi YA, Lin J, Mathialagan S, Tylaska L, Callegari E, Rodrigues AD, and Varma MVS (2018a) Role of Hepatic Organic Anion Transporter 2 in the Pharmacokinetics of R- and S-Warfarin: In Vitro Studies and Mechanistic Evaluation. *Mol Pharm* **15**:1284–1295.

Bi YA, Mathialagan S, Tylaska L, Fu M, Keefer J, Vildhede A, Costales C, Rodrigues AD, and Varma MVS (2018b) Organic Anion Transporter 2 Mediates Hepatic Uptake of Tolbutamide, a CYP2C9 Probe Drug. *J Pharmacol Exp Ther* **364**:390–398.

Chang JH, Ly J, Plise E, Zhang X, Messick K, Wright M, and Cheong J (2014) Differential effects of Rifampin and Ketoconazole on the blood and liver concentration of atorvastatin in wild-type and Cyp3a and Oatp1a/b knockout mice. *Drug Metab Dispos* **42**:1067–1073.

Chothe PP, Pemberton R, and Hariparsad N (2021) Function and Expression of Bile Salt Export Pump in Suspension Human Hepatocytes. *Drug Metab Dispos* **49**:314–321.

Chothe PP, Wu SP, Ye Z, and Hariparsad N (2018) Assessment of Transporter-Mediated and Passive Hepatic Uptake Clearance Using Rifamycin-SV as a Pan-Inhibitor of Active Uptake. *Mol Pharm* **15**:4677–4688.

Faessel H, Nemunaitis J, Bauer TM, Lockhart AC, Faller DV, Sedarati F, Zhou X, Venkatakrishnan K, and Harvey RD (2019) Effect of CYP3A inhibitors on the pharmacokinetics of pevonedistat in patients with advanced solid tumours. *Br J Clin Pharmacol* **85**:1464–1473.

Fan PW, Chen JZ, Allan Jaochico M, La H, Liu N, Mulder T, Cass RT, Durk M, Messick K, Valle N et al. (2016) Rate-Determining and Rate-Limiting Steps in the Clearance and Excretion of a Potent and Selective p21-Activated Kinase Inhibitor: A Case Study of Rapid Hepatic Uptake and Slow Elimination in Rat. *Drug Metab Lett* **10**:91–100.

Fujino R, Hashizume K, Aoyama S, Maeda K, Ito K, Toshimoto K, Lee W, Ninomiya SI, and Sugiyama Y (2018) Strategies to improve the prediction accuracy of hepatic intrinsic clearance of three antidiabetic drugs: Application of the extended clearance concept and consideration of the effect of albumin on CYP2C metabolism and OATP1B-mediated hepatic uptake. *Eur J Pharm Sci* **125**:181–192.

Hillgren KM, Keppler D, Zur AA, Giacomini KM, Stieger B, Cass CE, and Zhang L; International Transporter Consortium (2013) Emerging transporters of clinical importance: an update from the International Transporter Consortium. *Clin Pharmacol Ther* **94**:52–63.

Giacomini KM, Huang SM, Tweedie DJ, Benet LZ, Brouwer KL, Chu X, Dahlin A, Evers R, Fischer V, Hillgren KM, et al.; International Transporter Consortium (2010) Membrane transporters in drug development. *Nat Rev Drug Discov* **9**:215–236.

Ishiguro N, Maeda K, Kishimoto W, Saito A, Harada A, Ebner T, Roth W, Igarashi T, and Sugiyama Y (2006) Predominant contribution of OATP1B3 to the hepatic uptake of telmisartan, an angiotensin II receptor antagonist, in humans. *Drug Metab Dispos* **34**:1109–1115.

Khatri R, Fallon JK, Rementer RJB, Kulick NT, Lee CR, and Smith PC (2019) Targeted quantitative proteomic analysis of drug metabolizing enzymes and transporters by nano LC-MS/MS in the sandwich cultured human hepatocyte model. *J Pharmacol Toxicol Methods* **98**:106590.

Kimoto E, Mathialagan S, Tylaska L, Niosi M, Lin J, Carlo AA, Tess DA, and Varma MVS (2018) Organic Anion Transporter 2-Mediated Hepatic Uptake Contributes to the Clearance of High-Permeability-Low-Molecular-Weight Acid and Zwitterion Drugs: Evaluation Using 25 Drugs. *J Pharmacol Exp Ther* **367**:322–334.

Kunze A, Poller B, Huwyler J, and Camenisch G (2015) Application of the extended clearance concept classification system (ECCCS) to predict the victim drug-drug interaction potential of statins. *Drug Metab Pers Ther* **30**:175–188.

Liang X and Lai Y (2021) Overcoming the shortcomings of the extended-clearance concept: a framework for developing a physiologically-based pharmacokinetic (PBPK) model to select drug candidates involving transporter-mediated clearance. *Expert Opin Drug Metab Toxicol* **17**:869–886.

Lockhart AC, Bauer TM, Aggarwal C, Lee CB, Harvey RD, Cohen RB, Sedarati F, Nip TK, Faessel H, Dash AB, et al. (2019) Phase Ib study of pevonedistat, a NEDD8-activating enzyme inhibitor, in combination with docetaxel, carboplatin and paclitaxel, or gemcitabine, in patients with advanced solid tumors. *Invest New Drugs* **37**:87–97.

Lundquist P, Englund G, Skogastierna C, Lööf J, Johansson J, Hoogstraate J, Afzelius L, and Andersson TB (2014) Functional ATP-binding cassette drug efflux transporters in isolated human and rat hepatocytes significantly affect assessment of drug disposition. *Drug Metab Dispos* **42**:448–458.

Maeda K, Ikeda Y, Fujita T, Yoshida K, Azuma Y, Haruyama Y, Yamane N, Kumagai Y, and Sugiyama Y (2011) Identification of the rate-determining process in the hepatic clearance of atorvastatin in a clinical cassette microdosing study. *Clin Pharmacol Ther* **90**:575–581.

Miyauchi S, Masuda M, Kim SJ, Tanaka Y, Lee KR, Iwakado S, Nemoto M, Sasaki S, Shimono K, Tanaka Y, et al. (2018) The Phenomenon of Albumin-Mediated Hepatic Uptake of Organic Anion Transport Polypeptide Substrates: Prediction of the In Vivo Uptake Clearance from the In Vitro Uptake by Isolated Hepatocytes Using a Facilitated-Dissociation Model. *Drug Metab Dispos* **46**:259–267.

Pang KS, Han YR, Noh K, Lee PI, and Rowland M (2019) Hepatic clearance concepts and misconceptions: Why the well-stirred model is still used even though it is not physiologic reality? *Biochem Pharmacol* **169**:113596.

Patilea-Vrana GI and Unadkat JD (2018) When Does the Rate-Determining Step in the Hepatic Clearance of a Drug Switch from Sinusoidal Uptake to All Hepatobiliary Clearances? Implications for Predicting Drug-Drug Interactions. *Drug Metab Dispos* **46**:1487–1496.

Sato M, Toshimoto K, Tomaru A, Yoshikado T, Tanaka Y, Hisaka A, Lee W, and Sugiyama Y (2018) Physiologically Based Pharmacokinetic Modeling of Bosentan Identifies the Saturable Hepatic Uptake As a Major Contributor to Its Nonlinear Pharmacokinetics. *Drug Metab Dispos* **46**:740–748.

Shitara Y (2011) Clinical importance of OATP1B1 and OATP1B3 in drug-drug interactions. *Drug Metab Pharmacokinet* **26**:220–227.

Sohlenius-Sternbeck AK (2006) Determination of the hepatocellularity number for human, dog, rabbit, rat and mouse livers from protein concentration measurements. *Toxicol In Vitro* **20**:1582–1586.

Swords RT, Coutre S, Maris MB, Zeidner JF, Foran JM, Cruz J, Erba HP, Berdeja JG, Tam W, Vardhanabhuti S, et al. (2018) Pevonedistat, a first-in-class NEDD8-activating enzyme inhibitor, combined with azacitidine in patients with AML. *Blood* **131**:1415–1424.

Varma MV, Bi YA, Kimoto E, and Lin J (2014) Quantitative prediction of transporter- and enzyme-mediated clinical drug-drug interactions of organic anion-transporting polypeptide 1B1 substrates using a mechanistic net-effect model. *J Pharmacol Exp Ther* **351**:214–223.

Varma MV, Lai Y, Kimoto E, Goosen TC, El-Kattan AF, and Kumar V (2013) Mechanistic modeling to predict the transporter- and enzyme-mediated drug-drug interactions of repaglinide. *Pharm Res* **30**:1188–1199.

Wasan KM, Brocks DR, Lee SD, Sachs-Barrable K, and Thornton SJ (2008) Impact of lipoproteins on the biological activity and disposition of hydrophobic drugs: implications for drug discovery. *Nat Rev Drug Discov* **7**:84–99.

Watanabe T, Kusuhara H, Maeda K, Kanamaru H, Saito Y, Hu Z, and Sugiyama Y (2010) Investigation of the rate-determining process in the hepatic elimination of HMG-CoA reductase inhibitors in rats and humans. *Drug Metab Dispos* **38**:215–222.

Yoshikado T, Maeda K, Furihata S, Terashima H, Nakayama T, Ishigame K, Tsunemoto K, Kusuhara H, Furihata KI, and Sugiyama Y (2017) A Clinical Cassette Dosing Study for Evaluating the Contribution of Hepatic OATPs and CYP3A to Drug-Drug Interactions. *Pharm Res* **34**:1570–1583.

Zhang D, Hop CECA, Patilea-Vrana G, Gampa G, Seneviratne HK, Unadkat JD, Kenny JR, Nagapudi K, Di L, Zhou L, et al. (2019) Drug Concentration Asymmetry in Tissues and Plasma for Small Molecule-Related Therapeutic Modalities. *Drug Metab Dispos* **47**:1122–1135.

Zhou X, Sedarati F, Faller DV, Zhao D, Faessel HM, Chowdhury S, Bolleddula J, Li Y, Venkatakrishnan K, and Papai Z (2021) Phase I study assessing the mass balance, pharmacokinetics, and excretion of [^{14}C]-pevonedistat, a NEDD8-activating enzyme inhibitor in patients with advanced solid tumors. *Invest New Drugs* **39**:488–498.

Zhou X, Ke A, Burt H, Toneyama T, Yucha R, Chuang B, Pusalkar S, Chowdhury S, Sedarati F, Venkatakrishnan K, et al. (2021) Hepatic Uptake as a Rate-determining Step in Clearance: A Physiologically-based Pharmacokintic Model for Pevonedistat to Explore Mechanisms of Lack of Clinically-observed Drug-Drug Interactions with CYP3A Inhibitors & Inducers. Poster number-030. *Clin Pharmacol Drug Dev* **10** (S1):1–104 10.1002/cpdd.1004.

Address correspondence to: Dr. Paresh P. Chothe, Department of Drug Metabolism and Pharmacokinetics, 35 Landsdowne Street, Cambridge, MA 02139. E-mail: paresh.chothe@takeda.com

Journal: Drug Metabolism and Disposition

Manuscript ID: DMD-AR-2022-000836

Sinusoidal Uptake Determines the Hepatic Clearance of Pevonedistat (TAK-924) as Explained by Extended Clearance Model

Phil Sandoval, Bei-Ching Chuang, Lawrence Cohen, Tomoki Yoneyama, Sandeepraj Pusalkar[1], Robert W. Yucha, Swapan K Chowdhury[2] and Paresh P. Chothe*

Global Drug Metabolism and Pharmacokinetics, Takeda Development Center Americas, Inc. (TDCA), 95 Hayden Avenue, Lexington, Massachusetts, 02421, USA

[1]Current affiliation: Servier Pharmaceuticals, 200 Pier 4 Boulevard, Boston, Massachusetts, 02210, USA

[2]Current affiliation: Boston Pharmaceuticals, 55 Cambridge Parkway, Suite 400, Cambridge, Massachusetts, 02142, USA

Supplemental Figure 1: Uptake of Probe substrates and Validation of Reference Inhibitors of Hepatic Uptake Transporters

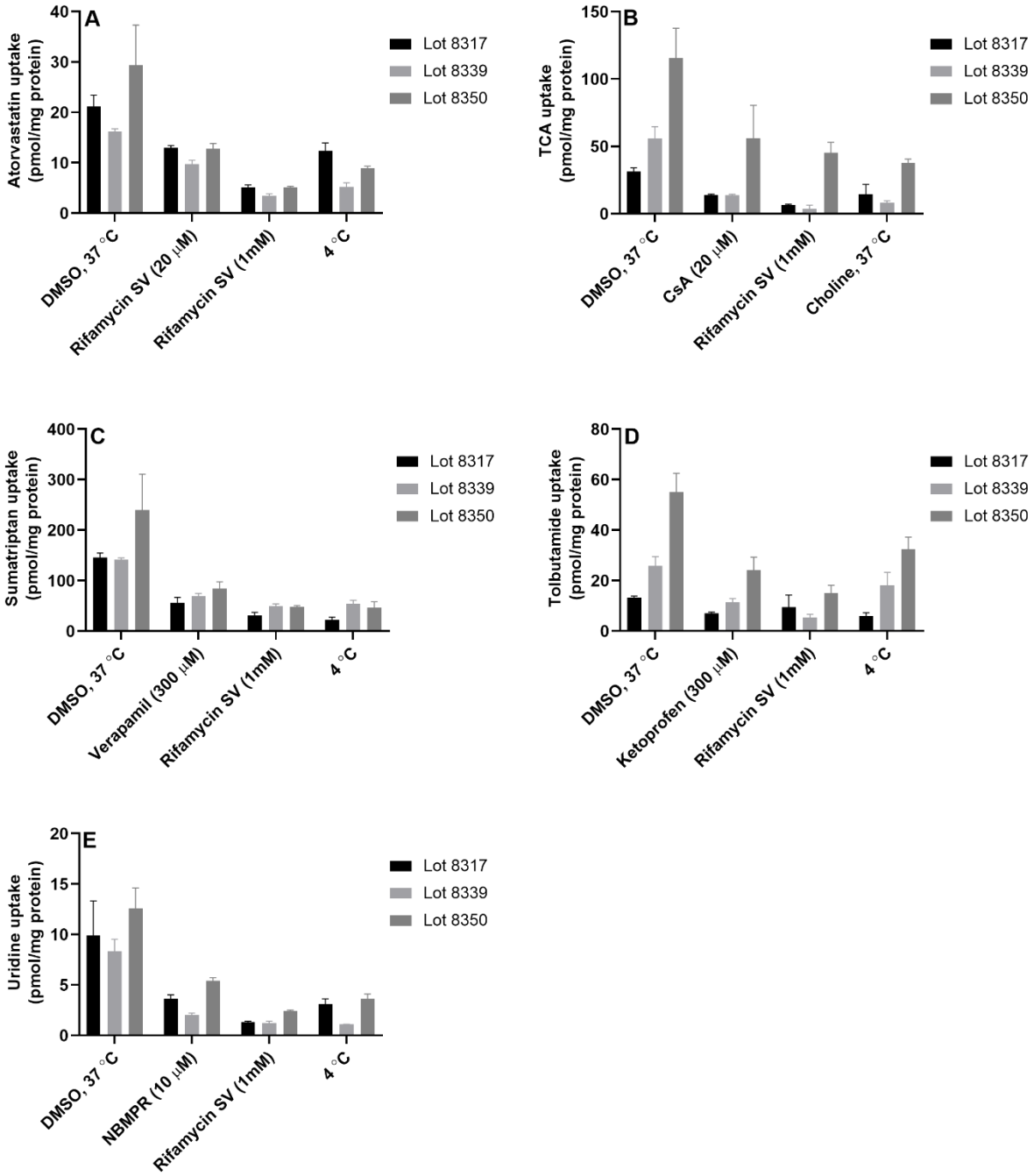

The uptake of atorvastatin (OATP substrate) was measured at 37 °C in the absence and presence of rifamycin SV (20 µM and 1mM) and at 4 °C (A), the uptake of TCA (NTCP substrate) was measured at 37 °C in KHB buffer with and without CsA (20 µM) and rifamycin SV (1mM) and in choline buffer (Na^+-free) (B), the uptake of sumatriptan (OCT1 substrate) was measured at 37 °C in the absence and presence of verapamil (300 µM) and rifamycin SV (1mM) and at 4 °C (C), the uptake of tolbutamide (OAT2 substrate) was measured at 37 °C in the absence and presence of ketoprofen (300 µM) and rifamycin SV (1mM) and at 4 °C (D) and the uptake of uridine (ENT1 substrate) was measured at 37 °C in the absence and presence of NBMPR (10 µM) and rifamycin SV (1mM) and at 4 °C (E) in plated human hepatocytes lot 8317, 8339 and 8350. The experiment was done in triplicates (n=3).

Supplemental Figure 2: The relationship of ESF on active uptake CL and predicted plasma CL of pevonedistat in humans

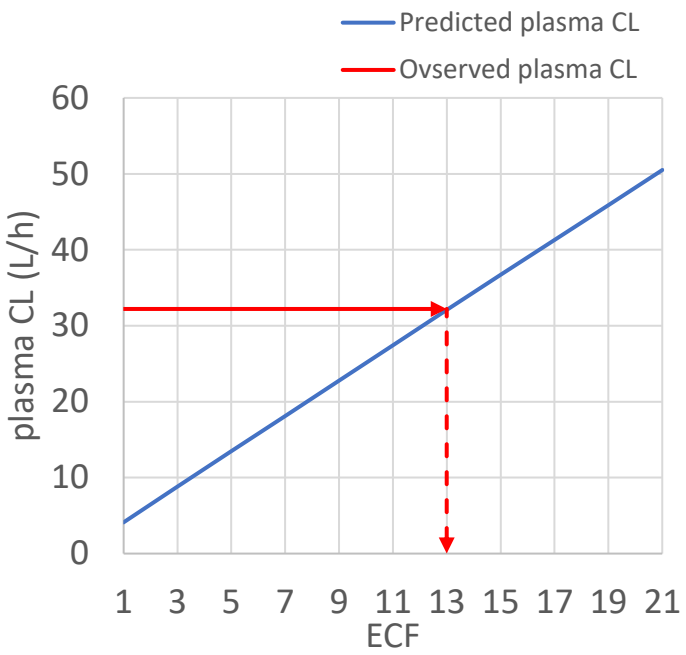

The relationship of ESF on active uptake CL and predicted plasma CL of pevonedistat monotherapy in humans (blue line). The Red horizontal arrow represents observed plasma CL, indicating that the observed plasma CL is reproduced by ESF of 13 (red dash arrow) by the ECM.

Supplemental Table 1: Demographic Information of Human Hepatocyte Donors

Donor ID	Sex	Age (year)	Race	Cause of death	BMI
1964	M	61	Caucasian	unknown	17.51
8280	M	55	Caucasian	Cardiovascular event	26.4
8317	M	59	Caucasian	Intracerebral hemorrhage	21.4
8339	F	31	African American	Asphyxiation	18.9
8350	M	26	Caucasian	Anoxia by Drug Intoxication	22.2